International Journal of Heat and Mass Transfer 53 (2010) 2434–2448

Contents lists available at ScienceDirect

International Journal of Heat and Mass Transfer

journal homepage: www.elsevier.com/locate/ijhmt

Laminar flow and convective heat transfer of non-Newtonian fluids in doubly connected ducts

Evaldiney R. Monteiro [a], Emanuel N. Macêdo [b], João N.N. Quaresma [b,*], Renato M. Cotta [c]

[a] Mining Engineering Department, Universidade Federal do Pará – CSSPA/UFPA, Marabá, PA, Brazil
[b] School of Chemical Engineering – Universidade Federal do Pará – FEQ/UFPA, Belém, PA, Brazil
[c] Laboratory of Transmission and Technology of Heat – LTTC, Mechanical Engineering Department – POLI-COPPE/UFRJ, Universidade Federal do Rio de Janeiro, Cx. Postal 68503 – Rio de Janeiro, RJ, 21945-970, Brazil

ARTICLE INFO

Article history:
Received 16 June 2009
Received in revised form 8 January 2010
Accepted 8 January 2010

Keywords:
Doubly connected ducts
Non-Newtonian flow
Thermally developing flow
Power-law fluids
Integral transforms

ABSTRACT

A hybrid numerical–analytical solution based on the Generalized Integral Transform Technique (GITT) is obtained for laminar heat and fluid flow of power-law non-Newtonian fluids inside doubly connected ducts. The mathematical formulation is constructed in the cylindrical coordinates system in such a way that the solid surfaces are described in terms of internal and external radii as functions of the angular coordinate, thus avoiding discontinuities in the boundary conditions. An annular doubly connected duct of arbitrary geometric configuration is considered for the analysis of the fully developed velocity field, as well as for the temperature field under thermally developing flow with boundary conditions of prescribed wall temperature. For illustration purposes, the case of eccentric annular ducts is more closely analyzed in order to demonstrate the ability of the GITT approach in dealing with such class of problems. Numerical results for the velocity field, the product of the Fanning friction factor-Reynolds number, temperature field and Nusselt numbers were produced for different values of the governing parameters, i.e., eccentricity, radii ratio and power-law indices. Such results were examined against previously reported ones, providing critical comparisons in order to illustrate the adequacy of the employed integral transform approach.

1. Introduction

Heat and fluid flow in doubly connected ducts is frequently found in a wide range of engineering and industrial applications in connection with heat exchange devices. Shah and London [1] pointed out a number of works that dealt with laminar flow inside annular passages and various other types of doubly connected geometries. Among them, elliptical ducts with central circular cores and eccentric annular ducts appear as the most relevant and frequently considered geometric configurations, mainly due their wide use in double-pipe type heat exchangers. On the other hand, the study of thermally developing flow in such configurations is important, mainly due to their usual employment in compact heat exchangers. In such type of thermal equipment, because of imperfections and tolerances in manufacturing, installation and operation, the eccentricity may or not be important, but there are a few applications where this effect is more pronounced and even promoted on purpose aimed at heat transfer enhancement. Oil and gas drilling wells, polymer and plastic extrusion process and nuclear reactors are some of the situations that reflect the importance of eccentricity. In addition, in dealing with purely viscous non-Newtonian fluids, heat and fluid flow analysis is commonly encountered in different industries. Chemical, food processing and pharmaceutical applications are just a few typical situations in which the power-law model can adequately describe the rheology of the working fluids.

The compilations in [1–3] provide extensive information on fully developed laminar flow of Newtonian fluids in ducts with doubly connected cross-sections. A variety of different methods has been employed in the literature to obtain solutions for the governing partial differential equations and associated boundary conditions, most based on discrete numerical techniques. Among the more analytically oriented contributions, one may cite the pioneering works of Piercy et al. [4], Sastry [5,6], Shivakumar [7] that employed conformal mapping methods, and Topakoglu and Arnas [8], which used an elliptical coordinates system to analyze the flow in confocal elliptical ducts. Solutions in closed-form were obtained by these authors for the velocity field and related flow characteristics. Shivakumar [7] also analyzed the flow in elliptical ducts with central circular cores through conformal mapping. Attention has also been devoted to the analysis of flow and heat transfer in eccentric annular ducts. The literature review brings up some of the earlier studies on such class of ducts, which are attributed to Piercy

* Corresponding author.
E-mail address: quaresma@ufpa.br (J.N.N. Quaresma).

0017-9310/$ - see front matter © 2010 Elsevier Ltd. All rights reserved.
doi:10.1016/j.ijheatmasstransfer.2010.01.040

Nomenclature

A_{ij}	coefficient defined by Eq. (20)
A_t	dimensionless parameter related to the cross-sectional area of the annular passage
B_i	coefficient defined by Eq. (21)
C_{ij}	coefficient defined by Eq. (22)
c_p	specific heat
D_h	hydraulic diameter
D_{ij}	coefficient defined by Eq. (23)
f	Fanning friction factor
h_{iw}, h_{ow}	local heat transfer coefficient at the inner and outer walls, respectively
k	thermal conductivity
K	consistency index of the fluid
L_i	normalization integral for the velocity field
L_1, L_2	radial characteristic length of the inner and outer surfaces, respectively
M_i	normalization integral for the temperature field in the R-direction
n	power-law index
N_ℓ	normalization integral for the temperature field in the θ-direction
NT, NT^*	truncations orders for the temperature expansion
Nu_{iw}, Nu_{ow}	local Nusselt number at the inner and outer walls, respectively
NV	truncation order for the velocity expansion
Pe	Peclet number
$P_{ij\ell m}$	coefficient defined by Eq. (66)
Pr	Prandtl number
$Q_{ij\ell m}$	coefficient defined by Eq. (67)
r, R	radial coordinates, dimensional and dimensionless, respectively
Re	Reynolds number
r_i, r_o	inner and outer radii of the eccentric annular duct, respectively
R_n	normalized radial coordinate
$\widetilde{\overline{T}}_{i\ell}$	transformed inlet temperature
r_1, R_1	functions that describe the inner surface, dimensional and dimensionless, respectively
r_2, R_2	functions that describe the outer surface, dimensional and dimensionless, respectively
T^*, T	temperature distributions, dimensional and dimensionless, respectively
T_e^*	inlet temperature
T_{iw}^*, T_{ow}^*	prescribed temperatures at the inner and outer walls, respectively
$\underline{T}_m$	dimensionless average temperature
$\overline{\overline{T}}_{i\ell}$	transformed potential for the temperature field
$v_{z,m}^*$, $V_{z,m}$	average flow velocity, dimensional and dimensionless, respectively
v_z^*, V_z	velocity distributions, dimensional and dimensionless, respectively
$\overline{V}_{z,i}$	transformed potential for the velocity field
z, Z	axial coordinates, dimensional and dimensionless, respectively

Greek letters

α	fluid thermal diffusivity
β_i	eigenvalues defined by Eq. (11)
γ	radii ratio
Γ_{ij}^*	eigenfunctions defined by Eq. (10)
ε^*, ε	eccentricities, dimensional and dimensionless, respectively
θ	angular coordinate
λ_i	eigenvalues defined by Eq. (56)
μ_ℓ	eigenvalues defined by Eq. (57)
ρ	density
Ψ_i	eigenfunctions defined by Eqs. (53) and (54)
Ω_ℓ	eigenfunctions defined by Eq. (55)

Subscripts and superscripts

i, j, k, ℓ, m	expansions indices
iw, ow	relative to the inner and outer wall, respectively
m	relative to average quantities
$-$, $\tilde{}$	integral transformed quantities

et al. [4], Stevenson [9], Snyder and Goldstein [10] and Jonsson and Sparrow [11] that concentrated their analyses on fluid flow only, while Cheng and Hwang [12], Trombetta [13] and Suzuki et al. [14] analyzed the heat transfer problem under different sets of boundary conditions. More recently, heat transfer in doubly connected ducts have regained interest in the works of Manglik and Fang [15], Fang et al. [16], Manglik and Fang [17], Escudier et al. [18], Coelho and Pinho [19], and Pinho and Coelho [20], in which the effects of eccentricity, duct rotation and viscous dissipation were investigated for the flow and heat transfer of Newtonian and non-Newtonian fluids as well. In addition, the recent work by Escudier et al. [18] offers the literature review on flow and heat transfer in eccentric annular ducts involving Newtonian and non-Newtonian fluids.

Within a wider framework, a hybrid analytical–numerical approach has been progressively advanced for the solution of convection–diffusion-type problems defined within irregular domains [21], and applied to the analysis of fully developed laminar flow within ducts of various shapes, such as trapezoidal, triangular, and hexagonal ducts [21–24], by extending the ideas on the Generalized Integral Transform Technique (GITT), as reviewed by Cotta [24,25] and Cotta and Mikhailov [26]. Laminar flow and heat transfer of Newtonian and non-Newtonian fluids inside irregular ducts of different geometric configurations was also treated in [27–33], again through extension of the GITT approach, yielding accurate numerical results for quantities of practical interest such as the Fanning friction factor and Nusselt numbers, within a wide range of the governing parameters.

Following this same line of research, the purpose of the present study is to solve the momentum and energy equations for laminar fully developed flow and thermally developing flow of non-Newtonian power-law fluids in doubly connected ducts by employing the GITT approach, and to provide reference results for the velocity field, the product of the Reynolds number-Fanning friction factor, temperature field and Nusselt numbers, for different values of the governing parameters according to the specific cross-section under consideration and thermal boundary conditions either at the inner or outer duct walls. The cylindrical coordinates system is used in the mathematical formulation, so that the solid surfaces are described in the form of internal and external radii as functions of the angular coordinate, and thus avoiding more involved formulations in other coordinates systems and cumbersome domain transformation approaches. The analysis is first accomplished in an arbitrary doubly connected duct in order to find a general solution for the velocity field and then for the temperature field. To illustrate the present approach, the case of eccentric annular ducts is considered, so as to demonstrate the ability of the GITT methodology in handling such class of problems. The thermal field is more

closely analyzed for the eccentric annular ducts subjected to constant temperatures either at the inner or outer duct walls. An analysis of convergence of the eigenfunction expansions is also performed and a set of reference results is established for quantities of practical interest, such as the product of the Reynolds number-Fanning friction factor, dimensionless average temperature and local Nusselt numbers, within a wide range of the dimensionless axial coordinate, for different power-law indices, radii ratios and dimensionless eccentricities. The present results are then critically compared with those previously reported in the literature.

2. Analysis

The present analysis is focused on the solution of the conservation equations for the laminar flow of non-Newtonian power-law fluids in doubly connected ducts by employing the GITT approach. First, the analysis is concerned with obtaining the velocity field for fully developed laminar flow, followed by the solution of the energy equation for thermally developing flow.

2.1. Velocity field

We consider fully developed laminar flow in the annular passage of a general doubly connected duct geometry, as described in Fig. 1. The cylindrical coordinates system is used to map the duct walls, so that the solid surfaces are described in terms of radii values as functions of the angular coordinate, thus avoiding discontinuities in the boundary conditions. In addition, it is taken into account that the flow is in steady state and incompressible with constant physical properties. Impermeability and no-slip conditions at the duct walls are also considered. The non-Newtonian viscosity expression $\eta = K\dot{\gamma}^{n-1}$ is described according to the Ostwald–de Waele model or power-law model [34], where K is the fluid consistency index, n is the power-law index and $\dot{\gamma}$ is the magnitude of the rate-of-deformation tensor. The power-law fluid classification is in general presented according to the n index value: pseudoplastic ($n < 1$), Newtonian ($n = 1$) and dilatant fluids ($n > 1$). Then, the mathematical formulation of the flow problem is given by the momentum conservation equation in the axial direction, in dimensionless form, as follows:

$$\frac{1}{R}\frac{\partial}{\partial R}\left[R\mu\frac{\partial V_z(R,\theta)}{\partial R}\right]+\frac{1}{R^2}\frac{\partial}{\partial\theta}\left[\mu\frac{\partial V_z(R,\theta)}{\partial\theta}\right]=-C,\quad \text{in}\quad R_1(\theta)<R<R_2(\theta),\ \ 0<\theta<2\pi \tag{1}$$

$$V_z(R_1(\theta),\theta)=0;\quad V_z(R_2(\theta),\theta)=0 \tag{2,3}$$

$$V_z(R,0)=V_z(R,2\pi);\quad \frac{\partial V_z(R,0)}{\partial\theta}=\frac{\partial V_z(R,2\pi)}{\partial\theta} \tag{4,5}$$

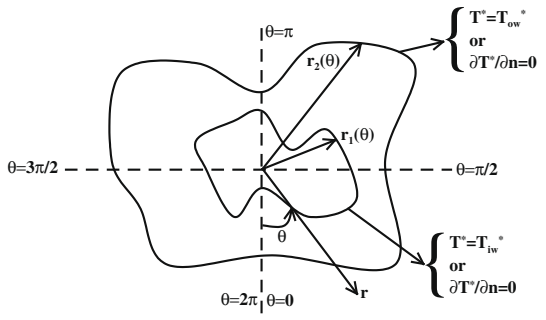

Fig. 1. Coordinates system and geometrical representation of a general doubly connected duct.

The following dimensionless variables were employed in the above formulation:

$$R=\frac{r}{L_2},\quad R_1(\theta)=\frac{r_1(\theta)}{L_2},\quad R_2(\theta)=\frac{r_2(\theta)}{L_2},$$

$$V_z(R,\theta)=\frac{v_z^*(r,\theta)}{\left[\left(-\frac{dp}{dz}\right)\frac{D_h^{n+1}}{K}\right]^{1/n}},\quad C=\left(\frac{L_2}{D_h}\right)^{n+1},$$

$$\mu=\left\{L_2^{n-1}\left[\left(-\frac{dp}{dz}\right)\frac{D_h^{n+1}}{K}\right]^{(1-n)/n}\right\}\left[\left(\frac{\partial v_z^*}{\partial r}\right)^2+\left(\frac{1}{r}\frac{\partial v_z^*}{\partial\theta}\right)^2\right]^{\frac{n-1}{2}}$$
$$=\left[\left(\frac{\partial V_z}{\partial R}\right)^2+\left(\frac{1}{R}\frac{\partial V_z}{\partial\theta}\right)^2\right]^{\frac{n-1}{2}} \tag{6}$$

where L_2 is a radial characteristic length of the outer surface, D_h is the hydraulic diameter of the duct and $r_1(\theta)$ and $r_2(\theta)$ are the functions of the polar angle that describe the radii of the inner and outer surfaces, respectively.

An analytical solution for the problem defined by Eqs. (1)–(5) is difficult to find in light of the irregular nature of the domain, given by the functions $R_1(\theta)$ and $R_2(\theta)$. In order to overcome this difficulty, the GITT approach will be employed in the hybrid numerical–analytical solution of the present formulation.

Following the ideas in [24–26], an appropriate auxiliary eigenvalue problem is selected, which shall provide the basis for the eigenfunction expansion. Here, due to the angular dependence of the boundaries, it is required to choose the radial coordinate R to provide the auxiliary eigenvalue problem and to be the coordinate that shall be eliminated in the integral transformation process. Therefore, the following eigenvalue problem is proposed:

$$\frac{1}{R}\frac{\partial}{\partial R}\left[R\frac{\partial\Gamma_i(R,\theta)}{\partial R}\right]+\beta_i^2(\theta)\frac{1}{R^2}\Gamma_i(R,\theta)=0,\quad \text{in}\ R_1(\theta)<R<R_2(\theta) \tag{7}$$

$$\Gamma_i(R_1(\theta),\theta)=0;\quad \Gamma_i(R_2(\theta),\theta)=0 \tag{8,9}$$

Eqs. (7)–(9) can be analytically solved to yield, respectively, the eigenfunctions and eigenvalues as:

$$\Gamma_i(R,\theta)=\sin\left\{\beta_i(\theta)\ln\left[\frac{R_2(\theta)}{R}\right]\right\};\quad \beta_i(\theta)=\frac{i\pi}{\ln\left[\frac{R_2(\theta)}{R_1(\theta)}\right]},\quad i=1,2,3,\ldots \tag{10,11}$$

It can be shown that the eigenfunctions $\Gamma_i(R,\theta)$ obey the following orthogonality property:

$$\int_{R_1(\theta)}^{R_2(\theta)}\frac{\Gamma_i(R,\theta)\Gamma_j(R,\theta)}{R}dR=\begin{cases}0, & i\neq j\\ L_i(\theta), & i=j\end{cases} \tag{12,13}$$

where $L_i(\theta)$ is the normalization integral determined as

$$L_i(\theta)=\int_{R_1(\theta)}^{R_2(\theta)}\frac{\Gamma_i^2(R,\theta)}{R}dR=\frac{1}{2}\ln\left[\frac{R_2(\theta)}{R_1(\theta)}\right] \tag{14}$$

Eqs. (7)–(9) together with the above orthogonality property allow the definition of the integral transform pair for the velocity field as:

$$\overline{V}_{z,i}(\theta)=\frac{1}{L_i(\theta)}\int_{R_1(\theta)}^{R_2(\theta)}\frac{\Gamma_i(R,\theta)V_z(R,\theta)}{R}dR,\quad \text{transform} \tag{15}$$

$$V_z(R,\theta)=\sum_{i=1}^{\infty}\Gamma_i(R,\theta)\overline{V}_{z,i}(\theta),\quad \text{inverse} \tag{16}$$

To obtain the resulting system of differential equations for the transformed potentials $\overline{V}_{z,i}(\theta)$, the partial differential equation (1) is multiplied by $\Gamma_i(R,\theta)/R$, integrated over the domain $[R_1(\theta), R_2(\theta)]$ in the R-direction, and the inverse formula, Eq. (16),

is employed in place of the velocity distribution $V_z(R,\theta)$, resulting in the following transformed ordinary differential system:

$$\sum_{j=1}^{\infty} A_{ij}(\theta)\frac{d^2\overline{V}_{z,j}}{d\theta^2} = B_i(\theta), \quad i = 1,2,3,\ldots \tag{17}$$

The same operation can be performed over the θ-direction boundary conditions given by Eqs. (4) and (5), to furnish:

$$\overline{V}_{z,i}(0) = \overline{V}_{z,i}(2\pi); \quad \frac{d\overline{V}_{z,i}(0)}{d\theta}L_i(0) + \sum_{j=1}^{\infty} C_{ij}\overline{V}_{z,j}(0) = \frac{d\overline{V}_{z,i}(2\pi)}{d\theta}L_i(2\pi) + \sum_{j=1}^{\infty} D_{ij}\overline{V}_{z,j}(2\pi) \tag{18,19}$$

where the coefficients in Eqs. (17)–(19) are defined as follows:

$$A_{ij}(\theta) = \int_{R_1(\theta)}^{R_2(\theta)} \frac{\Gamma_i(R,\theta)\Gamma_j(R,\theta)}{R}[I(R,\theta) + (n-1)F^2(R,\theta)J(R,\theta)/R^2]dR \tag{20}$$

$$\begin{aligned} B_i(\theta) = & -C\int_{R_1(\theta)}^{R_2(\theta)} R\Gamma_i(R,\theta)dR - \int_{R_1(\theta)}^{R_2(\theta)} \frac{\Gamma_i(R,\theta)}{R}[I(R,\theta) \\ & + (n-1)F^2(R,\theta)J(R,\theta)/R^2]H(R,\theta)dR - (n-1) \\ & \times \int_{R_1(\theta)}^{R_2(\theta)} \frac{\Gamma_i(R,\theta)}{R}E(R,\theta)F(R,\theta)G(R,\theta)J(R,\theta)dR \\ & + \int_{R_1(\theta)}^{R_2(\theta)} R\frac{\partial\Gamma_i(R,\theta)}{\partial R}E(R,\theta)I(R,\theta)dR \end{aligned} \tag{21}$$

$$C_{ij} = \int_{R_1(0)}^{R_2(0)} \frac{1}{R}\Gamma_i(R,0)\frac{\partial\Gamma_j(R,0)}{\partial\theta}dR; \qquad D_{ij} = \int_{R_1(2\pi)}^{R_2(2\pi)} \frac{1}{R}\Gamma_i(R,2\pi)\frac{\partial\Gamma_j(R,2\pi)}{\partial\theta}dR \tag{22,23}$$

$$E(R,\theta) = \sum_{k=1}^{\infty}\frac{\partial\Gamma_k(R,\theta)}{\partial R}\overline{V}_{z,k}(\theta);$$

$$F(R,\theta) = \sum_{k=1}^{\infty}\left[\frac{\partial\Gamma_k(R,\theta)}{\partial\theta}\overline{V}_{z,k}(\theta) + \Gamma_k(R,\theta)\frac{d\overline{V}_{z,k}(\theta)}{d\theta}\right] \tag{24,25}$$

$$G(R,\theta) = \sum_{k=1}^{\infty}\left[\frac{\partial^2\Gamma_k(R,\theta)}{\partial R\partial\theta}\overline{V}_{z,k}(\theta) + \frac{\partial\Gamma_k(R,\theta)}{\partial R}\frac{d\overline{V}_{z,k}(\theta)}{d\theta}\right] \tag{26}$$

$$H(R,\theta) = \sum_{k=1}^{\infty}\left[\frac{\partial^2\Gamma_k(R,\theta)}{\partial\theta^2}\overline{V}_{z,k}(\theta) + 2\frac{\partial\Gamma_k(R,\theta)}{\partial\theta}\frac{d\overline{V}_{z,k}(\theta)}{d\theta}\right] \tag{27}$$

$$I(R,\theta) = [E^2(R,\theta) + F^2(R,\theta)/R^2]^{(n-1)/2}; \qquad J(R,\theta) = [E^2(R,\theta) + F^2(R,\theta)R^2]^{(n-3)/2} \tag{28,29}$$

The coefficients $A_{ij}(\theta)$ and $B_i(\theta)$ depend on the transformed potentials and vary along θ, due to the nonlinear nature of the power-law rheological model and to the irregular domain of the duct in this angular direction, and need to be reevaluated along the numerical solution procedure. Eqs. (17)–(19) form an infinite nonlinear boundary value problem, which has to be truncated in a sufficiently high order *NV*, followed by computation of the transformed potentials of the velocity field, $\overline{V}_{z,i}(\theta)$, to within a user prescribed precision goal. For the solution of such a system, due to the expected stiff characteristics, specialized subroutines have to be employed, such as the subroutine DBVPFD from the IMSL Library [35]. This subroutine provides the important feature of automatic controlling the relative error over the solution of the ordinary differential equations system, allowing the user to establish error targets for the transformed potentials. Once this system is solved for the transformed potentials, the inverse formula, Eq. (16), is recalled to provide the velocity field.

In the realm of applications, related to pumping power requirements determination, one is concerned with quantities such as the product of the Fanning friction factor-Reynolds number, *fRe*. As a consequence, the average flow velocity is also required, which in dimensionless form can be obtained as:

$$V_{z,m} = \frac{v^*_{z,m}}{\left[\left(-\frac{dp}{dz}\right)\frac{D_h^{n+1}}{K}\right]^{1/n}} = \frac{\int_0^{2\pi}\int_{R_1(\theta)}^{R_2(\theta)} RV_z(R,\theta)dRd\theta}{\int_0^{2\pi}\int_{R_1(\theta)}^{R_2(\theta)} RdRd\theta} = \frac{1}{A_t(\gamma)}\int_0^{2\pi}\int_{R_1(\theta)}^{R_2(\theta)} RV_z(R,\theta)dRd\theta \tag{30}$$

where $A_t(\gamma)$ is a dimensionless parameter related to the cross-sectional area of the annular passage and it is a function of the radii ratio $\gamma = L_1/L_2$. Here L_1 is a radial characteristic length of the inner surface.

Applying the inverse formula, Eq. (16), into Eq. (30), the dimensionless average flow velocity is given by:

$$V_{z,m} = \frac{1}{A_t(\gamma)}\sum_{i=1}^{\infty} K_i; \quad K_i = \int_0^{2\pi}\int_{R_1(\theta)}^{R_2(\theta)} R\Gamma_i(R,\theta)\overline{V}_{Z,i}(\theta)dRd\theta \tag{31,32}$$

The Fanning friction factor and Reynolds number are defined as:

$$f = \left(-\frac{dp}{dz}\right)\frac{(D_h/4)}{\rho(v^*_{z,m})^2/2}; \quad Re = \frac{\rho(v^*_{z,m})^{2-n}D_h^n}{K} \tag{33,34}$$

Then, it is concluded that the product *fRe* is given as:

$$fRe = \frac{1}{2V^n_{z,m}} \tag{35}$$

2.2. Temperature field

Thermally developing flow of a power-law non-Newtonian fluid inside an arbitrary doubly connected duct is considered, also following the geometry and coordinates system in Fig. 1. The fully developed velocity profile described in the previous section is used as input for the present thermal problem formulation. In addition, the duct walls are subjected to different possibilities of boundary conditions, case A when the internal wall has a prescribed temperature condition and the external wall is insulated, while for case B the internal wall is insulated and the external wall is subjected to a uniform temperature. Therefore, the dimensionless energy equation for constant properties laminar flow, neglecting axial conduction and viscous dissipation, is written as:

$$W(R,\theta)\frac{\partial T(R,\theta,Z)}{\partial Z} = \frac{1}{R}\frac{\partial}{\partial R}\left[R\frac{\partial T(R,\theta,Z)}{\partial R}\right] + \frac{1}{R^2}\frac{\partial^2 T(R,\theta,Z)}{\partial\theta^2}, \quad \text{in } R_1(\theta) < R < R_2(\theta),\ 0 < \theta < 2\pi,\ Z > 0 \tag{36}$$

with inlet and boundary conditions given, respectively, as follows:

$$T(R,\theta,0) = 1, \quad R_1(\theta) \leqslant R \leqslant R_2(\theta), \quad 0 \leqslant \theta \leqslant 2\pi \tag{37}$$

$$\left.\begin{aligned} T(R_1(\theta),\theta,Z) = 0, \quad \frac{\partial T(R_2(\theta),\theta,Z)}{\partial\mathbf{n}} = 0, Z > 0, \quad \text{Case A} \\ \frac{\partial T(R_1(\theta),\theta,Z)}{\partial\mathbf{n}} = 0, \quad T(R_2(\theta),\theta,Z) = 0, Z > 0, \quad \text{Case B} \end{aligned}\right\} \tag{38—41}$$

$$T(R,0,Z) = T(R,2\pi,Z); \qquad \frac{\partial T(R,0,Z)}{\partial\theta} = \frac{\partial T(R,2\pi,Z)}{\partial\theta}, \quad Z > 0 \tag{42,43}$$

where $\partial/\partial\mathbf{n}$ represents the outward drawn normal derivative to the channel wall surface.

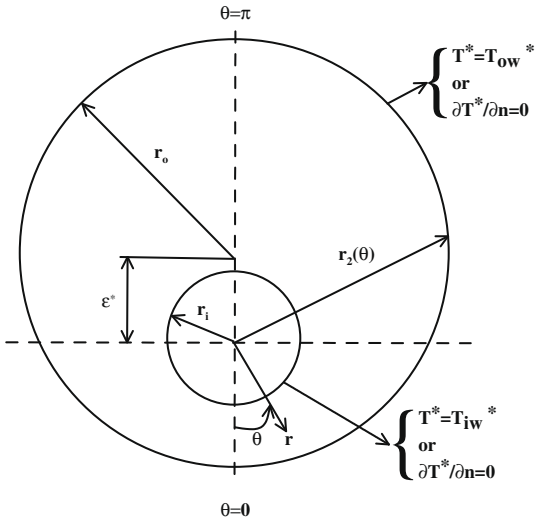

Fig. 2. Details of the eccentric annular duct analyzed.

Besides the dimensionless groups defined by Eqs. (6) and (34), the following ones were also employed in Eqs. (36)–(43):

$$Z=\frac{z}{D_h Pe},\quad Pe=RePr=\frac{v^*_{z,m}D_h}{\alpha}=\frac{\rho c_p}{k}v^*_{z,m}D_h,$$
$$Pr=\frac{K}{\rho(v^*_{z,m})^{1-n}D_h^{n-1}\alpha},\quad W(R,\theta)=\frac{V_z(R,\theta)}{V_{z,m}(D_h/L_2)^2},$$
$$\left.\begin{aligned}T(R,\theta,Z)&=\frac{T^*(r,\theta,z)-T^*_{iw}}{T^*_e-T^*_{iw}},\quad \text{Case A}\\ T(R,\theta,Z)&=\frac{T^*(r,\theta,z)-T^*_{ow}}{T^*_e-T^*_{ow}},\quad \text{Case B}\end{aligned}\right\}\tag{44}$$

Due to the non-separable nature of the velocity profile given in Eq. (36) and, consequently, of the related eigenvalue problem needed to solve the energy equation through analytical methods such as the Classical Integral Transform Technique (CITT) [36], an exact solution of problem given by Eqs. (36)–(43) is not feasible. On the other hand, with the advances on the GITT approach for the hybrid analytical–numerical solution of this class of non-transformable problem, it is possible to avoid these difficulties as now demonstrated. For this purpose, in order to alleviate the difficulties related to the non-separable eigenvalue problem, the following alternative auxiliary eigenvalue problems are chosen:

R-direction:

$$\frac{1}{R}\frac{\partial}{\partial R}\left[R\frac{\partial\Psi_i(R,\theta)}{\partial R}\right]+\frac{\lambda_i^2(\theta)}{R^2}\Psi_i(R,\theta)=0,\quad R_1(\theta)<R<R_2(\theta)\tag{45}$$

$$\left.\begin{aligned}&\Psi_i(R_1(\theta),\theta)=0,\quad \frac{\partial\Psi_i(R_2(\theta),\theta)}{\partial\mathbf{n}}=0,\quad \text{Case A}\\ &\frac{\partial\Psi_i(R_1(\theta),\theta)}{\partial\mathbf{n}}=0,\quad \Psi_i(R_2(\theta),\theta)=0,\quad \text{Case B}\end{aligned}\right\}\tag{46–49}$$

Table 1
Convergence behavior of the product *fRe* for eccentric annular ducts with different power-law indices, radii ratios and dimensionless eccentricities.

NV	*fRe*		
	$n=0.5$, $\gamma=0.8$, $\varepsilon=0.6$	$n=1$, $\gamma=0.5$, $\varepsilon=0.2$	$n=1.5$, $\gamma=0.2$, $\varepsilon=0$
5	5.5492	22.579	67.670
9	5.5391	22.549	67.099
13	5.5371	22.544	67.045
17	5.5364	22.543	67.049
21	5.5363	22.542	67.025
25	5.5363	22.542	67.017
29	5.5363	22.542	67.018
33	5.5364	22.542	67.017
37	5.5363	22.542	67.016

θ-direction:

$$\frac{d^2\Omega_\ell(\theta)}{d\theta^2}+\mu_\ell^2\Omega_\ell(\theta)=0,\quad 0<\theta<2\pi\tag{50}$$

$$\Omega_\ell(0)=\Omega_\ell(2\pi);\quad \frac{d\Omega_\ell(0)}{d\theta}=\frac{d\Omega_\ell(2\pi)}{d\theta}\tag{51,52}$$

which are readily solved to yield eigenfunctions and eigenvalues as follows:

$$\left.\begin{aligned}\Psi_i(R,\theta)&=\cos\left\{\lambda_i(\theta)\ln\left[\frac{R_2(\theta)}{R}\right]\right\},\quad \text{Case A}\\ \Psi_i(R,\theta)&=\sin\left\{\lambda_i(\theta)\ln\left[\frac{R_2(\theta)}{R}\right]\right\},\quad \text{Case B}\end{aligned}\right\};\quad \Omega_\ell(\theta)=\cos(\mu_\ell\theta)\tag{53–55}$$

$$\lambda_i(\theta)=\frac{(2i-1)\pi}{2}\frac{1}{\ln\left[\frac{R_2(\theta)}{R_1(\theta)}\right]},\quad i=1,2,3\ldots;\ \mu_\ell=\ell-1,\ \ell=1,2,3\ldots\tag{56,57}$$

Also, the eigenfunctions above obey the following orthogonality properties:

$$\int_{R_1(\theta)}^{R_2(\theta)}\frac{\Psi_i(R,\theta)\Psi_j(R,\theta)}{R}dR=\begin{cases}0, & i\neq j\\ M_i(\theta), & i=j\end{cases};$$
$$M_i(\theta)=\int_{R_1(\theta)}^{R_2(\theta)}\frac{\Psi_i^2(R,\theta)}{R}dR=\frac{1}{2}\ln\left[\frac{R_2(\theta)}{R_1(\theta)}\right]\tag{58,59}$$

Table 2
Comparison of the product *fRe* for eccentric annular ducts for the Newtonian case ($n=1$).

γ	*fRe*						
	$\varepsilon=0.05$	$\varepsilon=0.3$	$\varepsilon=0.4$	$\varepsilon=0.7$	$\varepsilon=0.8$	$\varepsilon=0.95$	$\varepsilon=1.0$
0.005	19.505[a]	18.845	18.380	16.802	16.352	15.901	15.843
	19.504[b]	18.844	18.380	16.802	16.352	15.900	15.842
0.01	20.004	19.222	18.674	16.833	16.309	15.770	15.690
	20.004	19.221	18.674	16.833	16.309	15.769	15.690
0.02	20.600	19.651	18.993	16.805	16.182	15.517	15.400
	20.600	19.650	18.993	16.805	16.182	15.517	15.399
0.03	20.993	19.919	19.179	16.738	16.042	15.278	15.127
	20.993	19.918	19.179	16.737	16.041	15.277	15.126
0.04	21.290	20.111	19.304	16.656	15.900	15.051	14.870
	21.289	20.110	19.304	16.656	15.900	15.051	14.869
0.05	21.528	20.259	19.393	16.569	15.761	14.837	14.628
	21.528	20.258	19.393	16.569	15.761	14.836	14.627
0.06	21.727	20.377	19.459	16.479	15.626	14.633	14.399
	21.726	20.376	19.459	16.479	15.625	14.633	14.399
0.08	22.045	20.554	19.548	16.301	15.369	14.257	13.979
	22.044	20.553	19.548	16.301	15.369	14.257	13.978
0.10	22.292	20.681	19.599	16.129	15.131	13.918	13.601
	22.292	20.680	19.599	16.129	15.131	13.917	13.600
0.15	22.731	20.878	19.647	15.739	14.610	13.199	12.809
	22.731	20.877	19.647	15.739	14.610	13.198	12.808
0.25	23.232	21.049	19.615	15.125	13.825	12.161	11.684
	23.231	21.048	19.615	15.125	13.825	12.161	11.683
0.30	23.387	21.087	19.583	14.887	13.529	11.781	11.277
	23.387	21.086	19.582	14.887	13.528	11.781	11.276
0.40	23.598	21.125	19.515	14.517	13.073	11.210	10.670
	23.598	21.125	19.515	14.517	13.073	11.210	10.669
0.60	23.811	21.144	19.415	14.075	12.537	10.551	9.9741
	23.811	21.144	19.415	14.075	12.537	10.551	9.973
0.70	23.861	21.146	19.386	13.955	12.392	10.375	9.7893
	23.861	21.145	19.386	13.955	12.392	10.375	9.788
0.90	23.906	21.145	19.358	13.844	12.258	10.213	9.6181
	23.908	21.145	19.358	13.843	12.258	10.213	9.617
1.00	23.910	21.145	19.355	13.833	12.245	10.197	9.6012
	23.910	21.145	19.355	13.833	12.245	10.196	9.600

[a] This work.
[b] Shah and London [1].

$$\int_0^{2\pi}\Omega_\ell(\theta)\Omega_m(\theta)d\theta=\begin{cases}0, & \ell\neq m\\ N_\ell, & \ell=m\end{cases};\quad N_\ell=\int_0^{2\pi}\Omega_\ell^2(\theta)d\theta=\begin{cases}2\pi, & \ell=1\\ \pi, & \ell>1\end{cases} \tag{60,61}$$

The eigenvalue problems given by Eqs. (45)–(49) and (50)–(52) allow the development of the following integral transform pair:

$$\widetilde{\overline{T}}_{i\ell}(Z)=\int_0^{2\pi}\int_{R1(\theta)}^{R_2(\theta)}\frac{\Psi_i(R,\theta)\Omega_\ell(\theta)T(R,\theta,Z)}{RM_i(\theta)N_\ell}dRd\theta,\quad \text{transform} \tag{62}$$

Table 3
Comparison of the product *fRe* for eccentric annular ducts for the non-Newtonian case.

γ	ε	*fRe*				
		n = 0.5	n = 0.8	n = 1	n = 1.2	n = 1.5
0.2	0	7.7187[a]	14.983[a]	23.088[a]	35.429[a]	67.017[a]
		7.7182[b]	14.982[b]	23.088[b]	35.429[b]	67.015[b]
		7.7196[e]	14.987[e]	23.088[c]	35.432[e]	66.997[e]
		7.7196[f]		23.100[e]		
	0.1	7.6757[a]	14.840[a]	22.830[a]	34.985[a]	66.063[a]
		7.7685[e]	14.848[e]	22.829[c]	34.987[e]	66.044[e]
		7.6770[f]		22.837[e]		
	0.2	7.5338[a]	14.434[a]	22.094[a]	33.726[a]	63.351[a]
		7.5423[e]	14.436[e]	22.093[c]	33.727[e]	63.338[e]
		7.5346[f]		22.102[e]		
	0.5	6.6385[a]	12.188[a]	18.197[a]	27.126[a]	49.280[a]
		6.6397[f]	12.192[d]	18.197[c]		
	0.6	6.2792[a]	11.346[a]	16.760[a]	24.723[a]	44.227[a]
		6.2840[e]	11.349[e]	16.760[c]	24.725[e]	44.221[e]
		6.2816[f]		16.764[e]		
	0.9	5.3337[a]	9.1741[a]	13.105[a]	18.692[a]	31.788[a]
		5.3330[f]		13.105[c]		
0.5	0	7.9417[a]	15.446[a]	23.813[a]	36.546[a]	69.129[a]
		7.9416[b]	15.446[b]	23.813[b]	36.546[b]	69.128[b]
		7.9395[e]	15.450[e]	23.813[c]	36.538[e]	69.086[e]
		7.9468[f]	15.438[f]	23.811[e]		
	0.1	7.8539[a]	15.244[a]	23.481[a]	36.009[a]	68.025[a]
		7.8600[e]	15.248[e]	23.481[c]	36.000[e]	67.983[e]
		7.8572[f]	15.236[f]	23.480[e]		
	0.2	7.5945[a]	14.671[a]	22.542[a]	34.481[a]	64.892[a]
		7.5978[e]	14.675[e]	22.541[c]	34.474[e]	64.852[e]
		7.5955[f]	14.663[f]	22.542[e]		
	0.5	6.2553[a]	11.724[a]	17.671[a]	26.529[a]	48.553[a]
		6.2605[f]	11.726[d]	17.671[c]		
			11.719[f]			
	0.6	5.7874[a]	10.665[a]	15.909[a]	23.647[a]	42.652[a]
		5.7909[e]	10.667[e]	15.909[c]	23.461[e]	42.727[e]
		5.7895[f]	10.659[f]	15.909[e]		
	0.9	4.5912[a]	7.9594[a]	11.422[a]	16.353[a]	27.929[a]
		4.5932[f]	7.9549[f]	11.422[c]		
0.8	0	7.9938[a]	15.554[a]	23.980[a]	36.804[a]	69.619[a]
		7.9938[b]	15.554[b]	23.980[b]	36.804[b]	69.617[b]
		7.9966[e]	15.557[e]	23.980[c]	36.794[e]	69.569[e]
		7.9994[f]		23.978[e]		
	0.1	7.8794[a]	15.332[a]	23.628[a]	36.242[a]	68.477[a]
		7.8880[e]	15.336[e]	23.627[c]	36.231[e]	68.429[e]
		7.8860[f]		23.626[e]		
	0.2	7.5676[a]	14.708[a]	22.631[a]	34.645[a]	65.237[a]
		7.5725[e]	14.711[e]	22.631[c]	34.635[e]	65.192[e]
		7.5704[f]		22.630[e]		
	0.5	6.0507[a]	11.533[a]	17.480[a]	26.329[a]	48.323[a]
		6.0548[f]	11.536[d]	17.480[c]		
	0.6	5.5363[a]	10.402[a]	15.622[a]	23.317[a]	42.208[a]
		5.5415[e]	10.405[e]	15.622[c]	23.309[e]	42.181[e]
		5.5399[f]		15.622[e]		
	0.9	4.2468[a]	7.5303[a]	10.903[a]	15.700[a]	26.952[a]
		4.2497[f]		10.903[c]		

[a] This work.
[b] Analytical solution.
[c] Shah and London [1].
[d] Fang et al. [16].
[e] Manglik and Fang [17].
[f] Escudier et al. [18].

$$T(R,\theta,Z)=\sum_{i=1}^{\infty}\sum_{\ell=1}^{\infty}\Psi_i(R,\theta)\Omega_\ell(\theta)\widetilde{\overline{T}}_{i\ell}(Z),\quad \text{inverse} \tag{63}$$

The next step in the GITT approach is the integral transformation process itself, when all independent variables are eliminated from the partial differential formulation but one, in this case the dimensionless axial coordinate. To obtain the resulting system of ordinary differential equations for the transformed potentials $\widetilde{\overline{T}}_{i\ell}(Z)$, the partial differential equation (36) is multiplied by $\Psi_i(R,\theta)\Omega_\ell(\theta)/[RM_i(\theta)N_\ell]$, integrated over the domains $[R_1(\theta), R_2(\theta)]$ in the R-direction and $[0, 2\pi]$ in the θ-direction, and the inverse formula, Eq. (63), is employed in place of the temperature distribution $T(R, \theta, Z)$, resulting, after some manipulation, in the following transformed ordinary differential system:

$$\sum_{j=1}^{\infty}\sum_{m=1}^{\infty}P_{ij\ell m}\frac{d\widetilde{\overline{T}}_{jm}(Z)}{dZ}+\sum_{j=1}^{\infty}\sum_{m=1}^{\infty}Q_{ij\ell m}\widetilde{\overline{T}}_{jm}(Z)=0,\quad Z>0,$$
$$j=1,2,3,\ldots\quad m=1,2,3,\ldots \tag{64}$$

$$\widetilde{\overline{T}}_{i\ell}(0)=\widetilde{\overline{r}}_{i\ell} \tag{65}$$

where

$$P_{ij\ell m}=\int_0^{2\pi}\int_{R_1(\theta)}^{R_2(\theta)}\frac{R\Psi_i(R,\theta)\Psi_j(R,\theta)\Omega_\ell(\theta)\Omega_m(\theta)W(R,\theta)}{M_i(\theta)N_\ell}dRd\theta \tag{66}$$

$$\begin{aligned}Q_{ij\ell m}=\mu_\ell^2\delta_{ij}\delta_{\ell m}+\delta_{ij}\int_0^{2\pi}\lambda_i^2(\theta)\frac{\Omega_\ell(\theta)\Omega_m(\theta)}{N_\ell}d\theta+w(-1)^{i+j}\\ \times\int_0^{2\pi}\frac{\Omega_\ell(\theta)\Omega_m'(\theta)}{M_i(\theta)N_\ell}\frac{R_1'(\theta)}{R_1(\theta)}d\theta+(w-1)\\ \times\int_0^{2\pi}\frac{\Omega_\ell(\theta)\Omega_m'(\theta)}{M_i(\theta)N_\ell}\frac{R_2'(\theta)}{R_2(\theta)}d\theta\\ -\int_0^{2\pi}\int_{R1(\theta)}^{R_2(\theta)}\left[\frac{\Psi_i(R,\theta)}{R}\frac{\partial^2\Psi_j(R,\theta)}{\partial\theta^2}\frac{\Omega_\ell(\theta)\Omega_m(\theta)}{M_i(\theta)N_\ell}\right]dRd\theta\\ -2\int_0^{2\pi}\int_{R1(\theta)}^{R_2(\theta)}\left[\frac{\Psi_i(R,\theta)}{R}\frac{\partial\Psi_j(R,\theta)}{\partial\theta}\frac{\Omega_\ell(\theta)\Omega_m'(\theta)}{M_i(\theta)N_\ell}\right]dRd\theta\end{aligned} \tag{67}$$

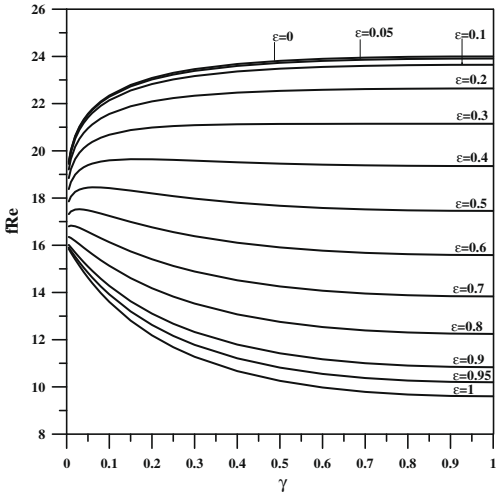

Fig. 3. Effect of radii ratio and eccentricity on the product *fRe* for n = 1.

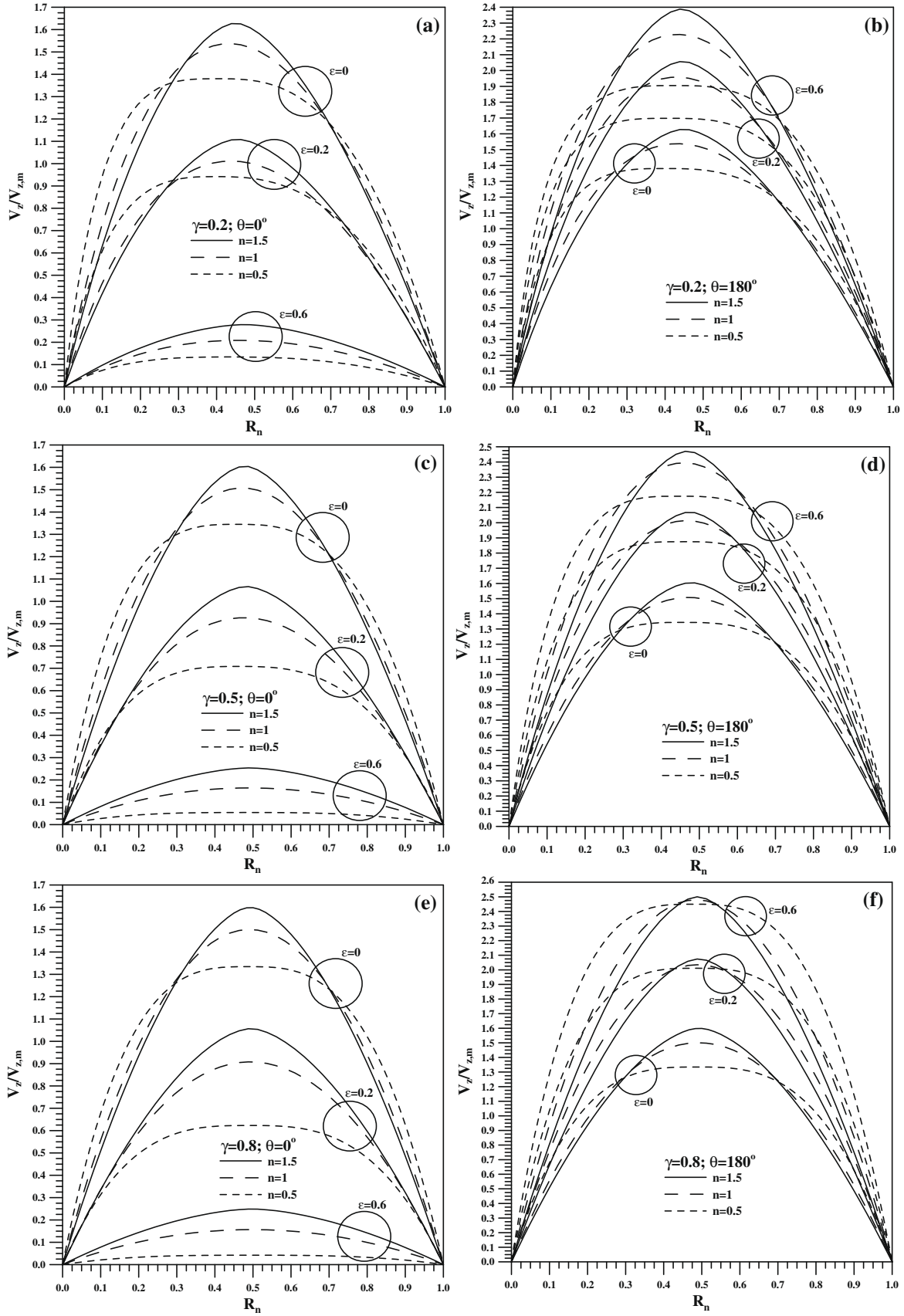

Fig. 4. Behavior of the velocity ratio for eccentric annular ducts: (a) $\gamma = 0.2$ and $\theta = 0^o$; (b) $\gamma = 0.2$ and $\theta = 180^o$; (c) $\gamma = 0.5$ and $\theta = 0^o$; (d) $\gamma = 0.5$ and $\theta = 180^o$; (e) $\gamma = 0.8$ and $\theta = 0^o$; and (f) $\gamma = 0.8$ and $\theta = 180^o$.

$$\widetilde{\overline{r}}_{i\ell} = \int_0^{2\pi} \int_{R_1(\theta)}^{R_2(\theta)} \frac{\Psi_i(R,\theta)\Omega_\ell(\theta)}{RM_i(\theta)N_\ell} dRd\theta;$$

$$\delta_{ij} = \begin{cases} 0, & i \neq j \\ 1, & i = j \end{cases}; \quad \delta_{\ell m} = \begin{cases} 0, & \ell \neq m \\ 1, & \ell = m \end{cases}; \quad w = \begin{cases} 0, & \text{Case A} \\ 1, & \text{Case B} \end{cases} \tag{68–71}$$

In Eq. (63) each summation is associated with the eigenfunction expansion in a corresponding spatial coordinate; for computational purposes, the series solution given by Eq. (63) is in general truncated to a finite number of terms in each summation, in order to compute the potential $T(R,\theta,Z)$. For best computational performance, it is advisable to implement a reordering scheme [37] to rewrite the double series in Eq. (63) into a single series form, by appropriately selecting the terms in the summations of more significant contribution to the final converged result, which leads to minimal sizes of the transformed differential system. The solution convergence is then verified by comparing the values for the potential obtained with the truncated series for increasing truncation orders. The coupled system of ordinary differential equations (64) may be analytically solved, as discussed in [24,27], or alternatively by efficient numerical algorithms for initial value problems, such as subroutine DIVPAG from the IMSL package [35], with high accuracy and automatic error control along the solution procedure. Here, the numerical approach was preferred aimed at constructing a more flexible algorithm for future use under more general simultaneously developing or nonlinear formulations [38]. Then, after the transformed potentials are numerically obtained, quantities of practical interest are determined from the analytical inverse formula (63), such as the dimensionless average temperature

$$T_m(Z) = \frac{1}{A_t(\gamma)} \int_0^{2\pi} \int_{R_1(\theta)}^{R_2(\theta)} \frac{RV_z(R,\theta)}{V_{z,m}} T(R,\theta,Z) dRd\theta \tag{72}$$

where, by introducing Eqs. (16) and (63), it results:

$$T_m(Z) = \frac{1}{A_t(\gamma)V_{z,m}} \sum_{i=1}^{\infty} \sum_{\ell=1}^{\infty} \sum_{n=1}^{\infty} S_{i\ell n} \widetilde{\overline{r}}_{i\ell}(Z); \quad S_{i\ell n} = \int_0^{2\pi} \int_{R_1(\theta)}^{R_2(\theta)} R\Psi_i(R,\theta)\Omega_\ell(\theta)\Gamma_n(R,\theta)\overline{V}_{z,n}(\theta) dRd\theta \tag{73,74}$$

The local Nusselt number can be calculated by making use of the temperature gradients at the walls integrated over the perimeter, to yield

$$Nu_{iw}(Z) = \frac{h_{iw}(z)D_h}{k} = -\frac{(D_h/L_2)}{2\pi} \frac{\int_0^{2\pi} \frac{\partial T(R_1(\theta),\theta)}{\partial \mathbf{n}} d\theta}{T_m(Z)};$$

$$Nu_{ow}(Z) = \frac{h_{ow}(z)D_h}{k} = 0, \quad \text{Case A} \tag{75,76}$$

$$Nu_{iw}(Z) = \frac{h_{iw}(z)D_h}{k} = 0;$$

$$Nu_{ow}(Z) = \frac{h_{ow}(z)D_h}{k} = -\frac{(D_h/L_2)}{2\pi} \frac{\int_0^{2\pi} \frac{\partial T(R_2(\theta),\theta)}{\partial \mathbf{n}} d\theta}{T_m(Z)}, \quad \text{Case B} \tag{77,78}$$

It is important to mention that for the cases where symmetry in the velocity and temperature fields at the angular positions $\theta = 0$ and $\theta = \pi$ prevails, such as for eccentric annular ducts, the boundary conditions given by Eqs. (4) and (5) and (42) and (43) may be rewritten as:

$$\frac{\partial V_z(R,0)}{\partial \theta} = 0; \quad \frac{\partial V_z(R,\pi)}{\partial \theta} = 0; \quad \frac{\partial T(R,0,Z)}{\partial \theta} = 0; \quad \frac{\partial T(R,\pi,Z)}{\partial \theta} = 0 \tag{79–81}$$

Table 4
Convergence behavior of the local Nusselt number expansions for eccentric annular ducts with different power-law indices, radii ratios and dimensionless eccentricities.

$NT = NT^*$	Nu(Z)					
	Case A			Case B		
	$n = 0.5$, $\gamma = 0.8$, $\varepsilon = 0.6$	$n = 1$, $\gamma = 0.5$, $\varepsilon = 0.2$	$n = 1.5$, $\gamma = 0.2$, $\varepsilon = 0$	$n = 0.5$, $\gamma = 0.8$, $\varepsilon = 0.6$	$n = 1$, $\gamma = 0.5$, $\varepsilon = 0.2$	$n = 1.5$, $\gamma = 0.2$, $\varepsilon = 0$
	$Z = 10^{-4}$					
5	14.930	22.371	32.954	12.930	13.363	9.8819
10	20.155	30.131	32.183	17.574	21.918	16.946
15	22.365	28.561	31.832	20.088	25.494	22.212
20	22.737	27.823	31.792	21.212	25.914	25.009
25	22.356	27.844	31.793	21.462	25.435	25.594
30	21.966	27.840	31.785	21.274	24.942	25.001
35	21.806	27.826	31.785	20.986	24.686	24.287
40	21.790	27.816	31.782	20.776	24.608	23.907
	$Z = 10^{-2}$					
5	3.9667	7.0572	9.8155	3.5942	5.6492	5.4891
10	3.8732	7.0378	9.7023	3.5322	5.5630	5.4225
15	3.8718	7.0407	9.7149	3.5251	5.5580	5.4088
20	3.8705	7.0393	9.7106	3.5233	5.5565	5.4058
25	3.8704	7.0397	9.7125	3.5227	5.5561	5.4048
30	3.8701	7.0394	9.7115	3.5224	5.5559	5.4043
35	3.8701	7.0394	9.7121	3.5223	5.5558	5.4041
40	3.8701	7.0394	9.7117	3.5222	5.5556	5.4039
	$Z = 1$					
5	1.2594	3.7054	8.0802	1.1370	2.8766	4.2089
10	1.2517	3.7051	8.0787	1.1299	2.8766	4.2087
15	1.2517	3.7051	8.0787	1.1299	2.8766	4.2087
20	1.2517	3.7051	8.0787	1.1299	2.8766	4.2087
25	1.2517	3.7051	8.0787	1.1299	2.8766	4.2087
30	1.2517	3.7051	8.0787	1.1299	2.8766	4.2087
35	1.2517	3.7051	8.0787	1.1299	2.8766	4.2087
40	1.2517	3.7051	8.0786	1.1299	2.8766	4.2087

3. Results and discussion

Eccentric annular ducts are considered in the present analysis for illustration of the proposed approach in handling laminar flow and convective heat transfer of non-Newtonian fluids in doubly connected ducts, as described by the geometry and coordinates systems in Fig. 2. The parameters related to the geometric configuration of such doubly connected duct are: $A_f(\gamma) = \pi(1-\gamma^2)$, $D_h = 2r_o(1-\gamma)$, $L_1 = r_i$, $L_2 = r_o$, $R_1(\theta) = \gamma$, $R_2(\theta) = [1-\varepsilon^2(1-\gamma)^2\sin^2\theta]^{1/2} - \varepsilon(1-\gamma)\cos\theta$, which were previously defined, and the additional parameter that appears in these definitions is the dimensionless eccentricity of the annular duct stated as $\varepsilon = \varepsilon^*/(r_o - r_i)$.

3.1. Velocity field

Numerical results for the product of the Fanning friction factor-Reynolds number and for the velocity field inside eccentric annular ducts were obtained from a code developed in the FORTRAN 90 programming language. The code was implemented on a PENTIUM IV Core 2 Duo E7400 2.8 GHz microcomputer, and the system given by Eqs. (17)–(19) was handled through the subroutine DBVPFD from the IMSL Library [35]. A relative error target of 10^{-5} was employed throughout the computations, for varying values of the power-law index, n, and of the geometric parameters, radii ratio, γ, and dimensionless eccentricity, ε. A typical CPU running time for the computations such as those shown in Table 1 is about 300 s.

First, a convergence behavior analysis for the product of the Fanning friction factor-Reynolds number, *fRe*, is shown in Table 1, for the cases $n = 0.5$, $\gamma = 0.8$, $\varepsilon = 0.6$; $n = 1$, $\gamma = 0.5$, $\varepsilon = 0.2$ and $n = 1.5$, $\gamma = 0.2$, $\varepsilon = 0$. In all computations a maximum truncation order of $NV = 37$ in the velocity expansion was employed, and excellent convergence rates are clearly observable, with full convergence to four digits being achieved for the case $n = 0.5$, $\gamma = 0.8$, $\varepsilon = 0.6$, even for lower truncation orders (approximately $NV = 17$). For $n = 1$, $\gamma = 0.5$, $\varepsilon = 0.2$ five digits are reached with a truncation order of around $NV \approx 21$, and for the case $n = 1.5$, $\gamma = 0.2$, $\varepsilon = 0$ a convergence to four digits is verified with $NV \approx 25$ terms. Therefore, after this convergence analysis, the subsequent computations were performed using up to 37 terms ($NV \leqslant 37$) in the velocity eigenfunction expansion.

Table 2 brings a set of integral transform results for eccentric annular ducts in the case of Newtonian fluids ($n = 1$) together with a comparison against numerical results presented by Shah and London [1]. An excellent agreement is thus verified in a wide range of governing parameters. In general, an increase in the radii ratio, γ, results in increasing *fRe* in light of the reduction in the cross-section of the annular duct. On the other hand, the increase of ε diminishes the product *fRe*, basically due to an increase in the dimensionless average velocity.

A set of reference results for the product *fRe* is shown in Table 3 for power-law non-Newtonian fluids, with different power-law indices, and different geometric parameters γ and ε. Also, this table furnishes a comparison of the present results with those from the analytical solution for the case of null eccentricity, as well as against those results of Shah and London [1], Manglik and Fang [17] and Escudier et al. [18]. In general, an excellent agreement was achieved among the present results and those from the analytical solution in Shah and London [1], and a good agreement also with results from references [17] and [18], with roughly three digits of adherence. From Table 3 it can also be observed that for higher power-law indices there is an increase of the product *fRe* in light of the friction increase at the duct wall, due to the increase in the apparent viscosity of the fluid that results in higher local velocity gradient regions. An inverse trend is observed in relation to the influence of the eccentricity on the product *fRe*, which suffers a

Table 5a
Comparison of the present results for asymptotic Nusselt number for eccentric annular ducts against previously reported results (Case A).

γ	ε	Nu_∞				
		Case A				
		$n = 0.5$	$n = 0.8$	$n = 1$	$n = 1.2$	$n = 1.5$
0.2	0	8.1671[a]	8.1511[a]	8.1296[a]	8.1079[a]	8.0786[a]
		8.1672[b]	8.1511[b]	8.1296[b]	8.1079[b]	8.0787[b]
		8.1093[c]	8.0860[c]	8.0651[c]	8.0436[c]	8.0151[c]
	0.1	7.6315[a]	7.5751[a]	7.5609[a]	7.5522[a]	7.5427[a]
		7.5648[c]	7.5123[c]	7.4987[c]	7.4904[c]	7.4812[c]
	0.2	6.5725[a]	6.5308[a]	6.5300[a]	6.5363[a]	6.5479[a]
		6.5244[c]	6.4952[c]	6.4861[c]	6.4668[c]	6.4574[c]
	0.5	4.3072[a]	4.3223[a]	4.3304[a]	4.3384[a]	4.3493[a]
	0.6	3.8757[a]	3.8855[a]	3.8901[a]	3.8947[a]	3.9003[a]
		3.9761[c]	3.9868[c]	3.9915[c]	3.9956[c]	4.0012[c]
	0.9	2.9574[a]	2.9507[a]	2.9484[a]	2.9456[a]	2.9420[a]
0.5	0	5.7696[a]	5.7517[a]	5.7381[a]	5.7257[a]	5.7099[a]
		5.7696[b]	5.7517[b]	5.7381[b]	5.7257[b]	5.7099[b]
		5.7621[c]	5.7450[c]	5.7316[c]	5.7195[c]	5.7040[c]
	0.1	4.5880[a]	4.6605[a]	4.6985[a]	4.7260[a]	4.7535[a]
		4.5929[c]	4.6677[c]	4.7059[c]	4.7331[c]	4.7606[c]
	0.2	3.5405[a]	3.6490[a]	3.7051[a]	3.7474[a]	3.7930[a]
		3.5666[c]	3.6826[c]	3.7386[c]	3.7809[c]	3.8264[c]
	0.5	2.1299[a]	2.1932[a]	2.2264[a]	2.2537[a]	2.2857[a]
	0.6	1.9168[a]	1.9600[a]	1.9843[a]	2.0042[a]	2.0289[a]
		2.0338[c]	2.0790[c]	2.1039[c]	2.1250[c]	2.1504[c]
	0.9	1.5175[a]	1.5297[a]	1.5374[a]	1.5445[a]	1.5537[a]
0.8	0	5.1095[a]	5.0919[a]	5.0819[a]	5.0738[a]	5.0639[a]
		5.1096[b]	5.0919[b]	5.0820[b]	5.0738[b]	5.0639[b]
		5.1051[c]	5.0881[c]	5.0785[c]	5.0702[c]	5.0604[c]
	0.1	3.5093[a]	3.6723[a]	3.7318[a]	3.7710[a]	3.8113[a]
		3.5196[c]	3.6819[c]	3.7409[c]	3.7806[c]	3.8202[c]
	0.2	2.5551[a]	2.7410[a]	2.8160[a]	2.8688[a]	2.9230[a]
		2.5701[c]	2.7616[c]	2.8369[c]	2.8897[c]	2.9443[c]
	0.5	1.4139[a]	1.5217[a]	1.5708[a]	1.6078[a]	1.6480[a]
	0.6	1.2517[a]	1.3373[a]	1.3773[a]	1.4078[a]	1.4414[a]
		1.2923[c]	1.3804[c]	1.4216[c]	1.4529[c]	1.4874[c]
	0.9	0.96176[a]	1.0095[a]	1.0328[a]	1.0510[a]	1.0713[a]

[a] This work.
[b] Analytical solution for $\varepsilon = 0$ based on Refs. [39,40].
[c] Manglik and Fang [17].

Table 5b
Comparison of the present results for asymptotic Nusselt number for eccentric annular ducts against previously reported results (Case B).

γ	ε	Nu_∞				
		Case B				
		$n = 0.5$	$n = 0.8$	$n = 1$	$n = 1.2$	$n = 1.5$
0.2	0	4.2287[a]	4.1954[a]	4.1944[a]	4.1988[a]	4.2087[a]
		4.2287[b]	4.1954[b]	4.1944[b]	4.1988[b]	4.2087[b]
	0.1	4.0259[a]	3.9525[a]	3.9468[a]	3.9521[a]	3.9662[a]
	0.2	3.5912[a]	3.5034[a]	3.4937[a]	3.4986[a]	3.5151[a]
	0.5	2.6930[a]	2.6176[a]	2.5979[a]	2.5896[a]	2.5877[a]
	0.6	2.5643[a]	2.4823[a]	2.4570[a]	2.4430[a]	2.4335[a]
	0.9	2.3494[a]	2.2449[a]	2.2062[a]	2.1798[a]	2.1537[a]
0.5	0	4.4534[a]	4.4330[a]	4.4293[a]	4.4284[a]	4.4293[a]
		4.4535[b]	4.4330[b]	4.4293[b]	4.4284[b]	4.4294[b]
	0.1	3.5620[a]	3.6059[a]	3.6394[a]	3.6675[a]	3.6999[a]
	0.2	2.7615[a]	2.8308[a]	2.8766[a]	2.9145[a]	2.9587[a]
	0.5	1.7008[a]	1.7336[a]	1.7580[a]	1.7808[a]	1.8101[a]
	0.6	1.5484[a]	1.5644[a]	1.5808[a]	1.5974[a]	1.6198[a]
	0.9	1.2787[a]	1.2672[a]	1.2686[a]	1.2725[a]	1.2803[a]
0.8	0	4.7097[a]	4.6916[a]	4.6849[a]	4.6805[a]	4.6760[a]
		4.7097[b]	4.6916[b]	4.6850[b]	4.6805[b]	4.6761[b]
	0.1	3.2233[a]	3.3713[a]	3.4131[a]	3.4643[a]	3.5058[a]
	0.2	2.3367[a]	2.5050[a]	2.5751[a]	2.6254[a]	2.6780[a]
	0.5	1.2796[a]	1.3756[a]	1.4208[a]	1.4557[a]	1.4942[a]
	0.6	1.1299[a]	1.2054[a]	1.2422[a]	1.2709[a]	1.3032[a]
	0.9	0.86311[a]	0.90385[a]	0.92516[a]	0.94243[a]	0.96214[a]

[a] This work.
[b] Analytical solution for $\varepsilon = 0$ based on Refs. [39,40].

reduction as this parameter increases. The influence of the two geometric parameters is better inspected from Fig. 3, which presents the variation of *fRe* with both the eccentricity and the aspect ratio, for the Newtonian fluid situation. It should be noted that for a fixed aspect ratio, varying the eccentricity does not alter the flow area, but essentially moves one cylindrical wall with respect to the other one. Increasing the eccentricity is then confirmed to monotonically decrease the product *fRe*.

Fig. 4 shows plots of the velocity ratio $V_z/V_{z,m}$ at $\theta = 0^o$ and $\theta = 180^o$ as a function of the normalized radial coordinate, $R_n = [R - R_1(\theta)]/[R_2(\theta) - R_1(\theta)]$, for different power-law indices, eccentricities and radii ration. Higher power-law indices present more pronounced velocity peaks and reduced velocities closer to the walls at both opposing angular positions, due to the increased apparent viscosity. It is observed that an increase in the radii ratio tends to make the velocity field less asymmetrical across the normalized radial coordinate, while increasing the eccentricity causes an opposite effect at the two angular positions analyzed, due to the more marked differences in shape between the two flow passages. For $\theta = 0^o$, as the eccentricity increases, the velocity maximum tends to diminish, with the decreased radial distance between the two walls that increases the flow resistance; on the other hand, at $\theta = 180^o$, the opposite behavior is verified, i.e., the velocity peak increases within this wider flow path.

3.2. Temperature field

Once the velocity field is available, the system given by Eqs. (64) and (65) for the temperature field is handled through the subroutine DIVPAG from the IMSL package [35], here with a user-prescribed relative error target of 10^{-8} on the transformed temperatures. Numerical results for thermally developing laminar flow of power-law fluids inside eccentric annular ducts were obtained through the code developed in the FORTRAN 90 programming language, which was also implemented on a PENTIUM IV Core 2 Duo E7400 2.8 GHz microcomputer. The results are presented in terms of dimensionless average temperatures and local Nusselt numbers along the dimensionless axial coordinate, within the range $Z = 10^{-4}$–1, for different values of power-law indices,

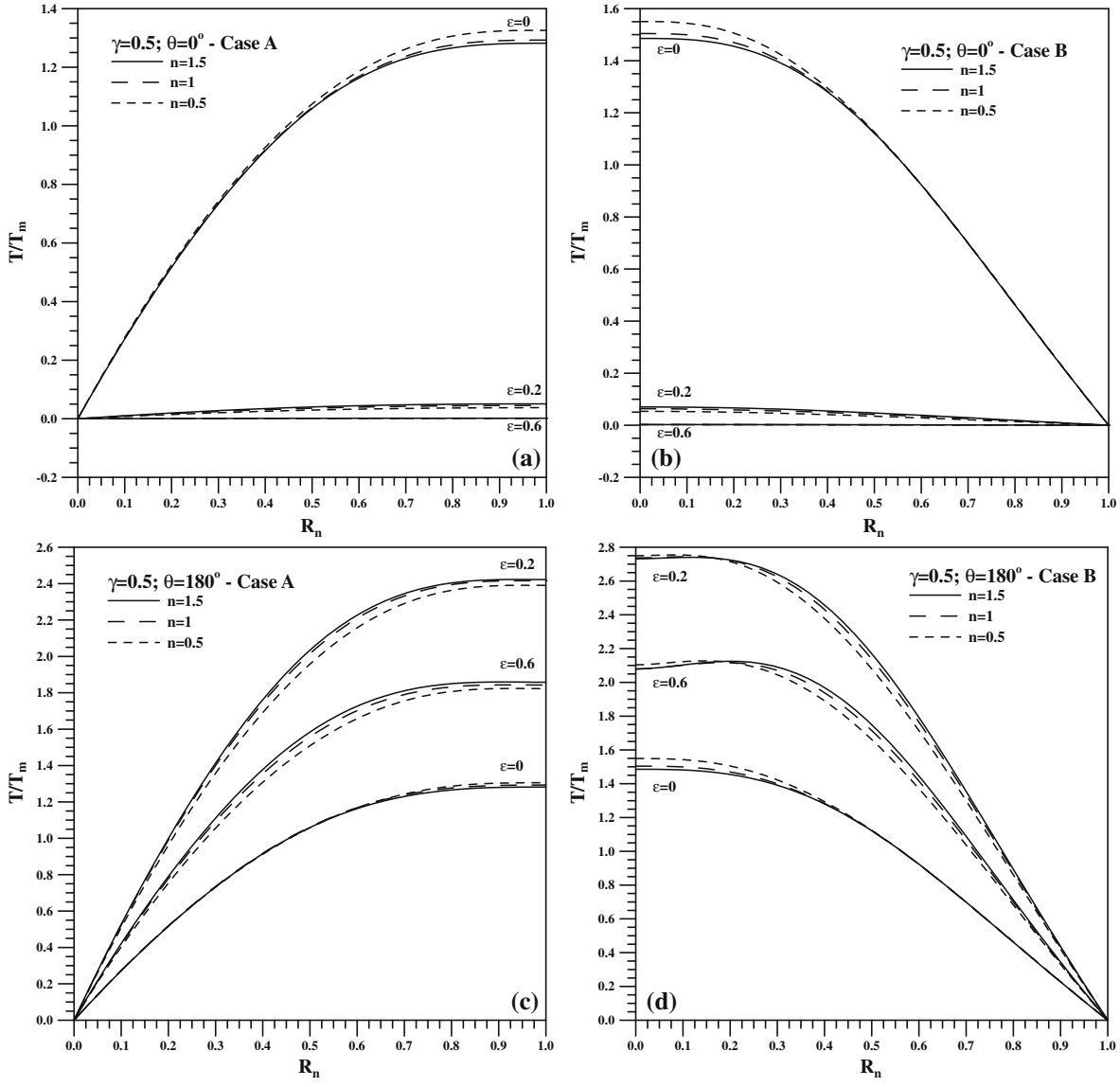

Fig. 5. Behavior of the temperature ratio for eccentric annular ducts: (a) $\gamma = 0.5$ and $\theta = 0^o$ – Case A; (b) $\gamma = 0.5$ and $\theta = 0^o$ – Case B; (c) $\gamma = 0.5$ and $\theta = 180^o$ – Case A; and (d) $\gamma = 0.5$ and $\theta = 180^o$ – Case B.

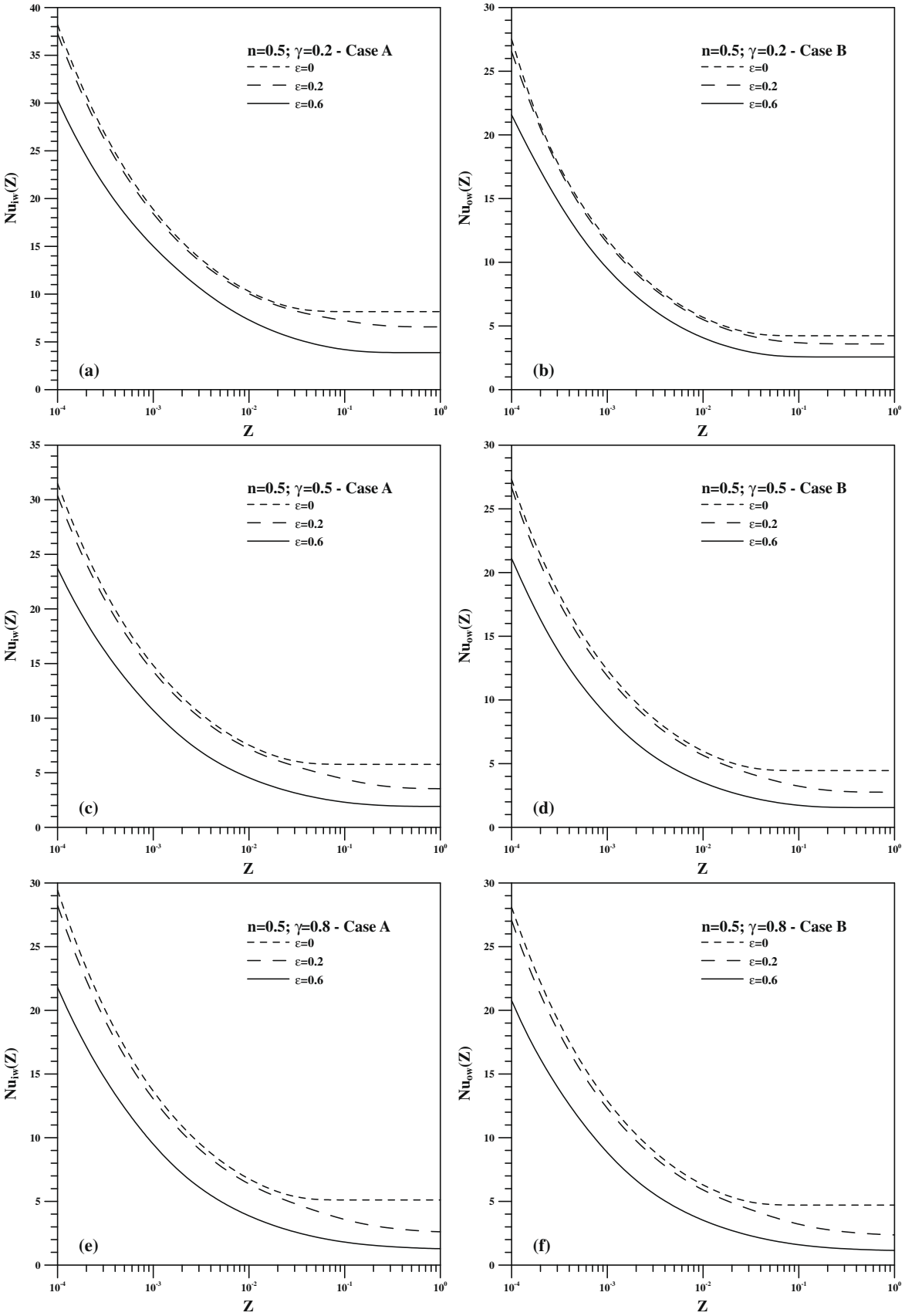

Fig. 6. Evolution of the local Nusselt number along the thermal entry region for $n = 0.5$ and different eccentricities: (a) $\gamma = 0.2$ – Case A; (b) $\gamma = 0.2$ – Case B; (c) $\gamma = 0.5$ – Case A; (d) $\gamma = 0.5$ – Case B; (e) $\gamma = 0.8$ – Case A; and (f) $\gamma = 0.8$ – Case B.

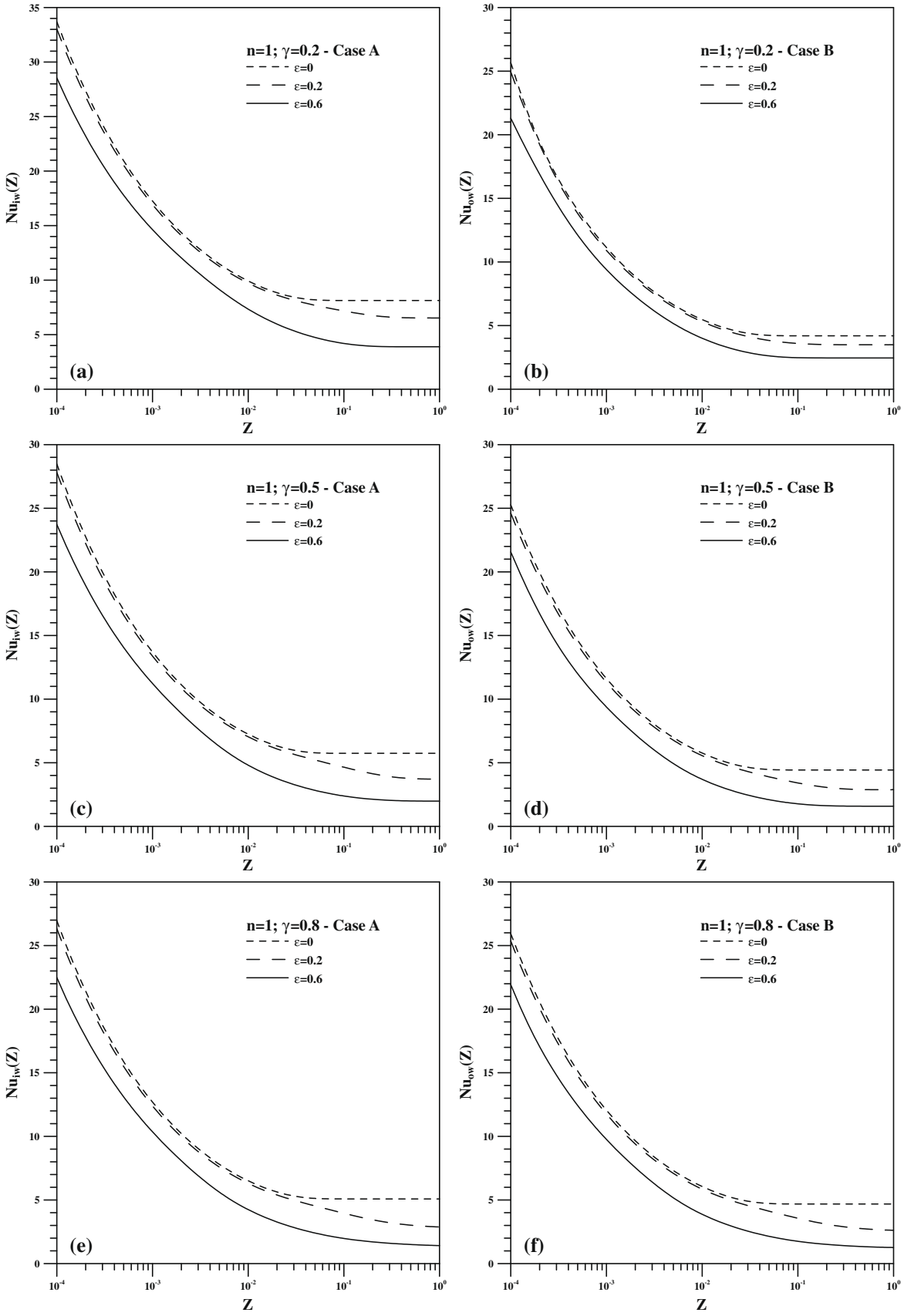

Fig. 7. Evolution of the local Nusselt number along the thermal entry region for $n = 1$ and different eccentricities: (a) $\gamma = 0.2$ – Case A; (b) $\gamma = 0.2$ – Case B; (c) $\gamma = 0.5$ – Case A; (d) $\gamma = 0.5$ – Case B; (e) $\gamma = 0.8$ – Case A; and (f) $\gamma = 0.8$ – Case B.

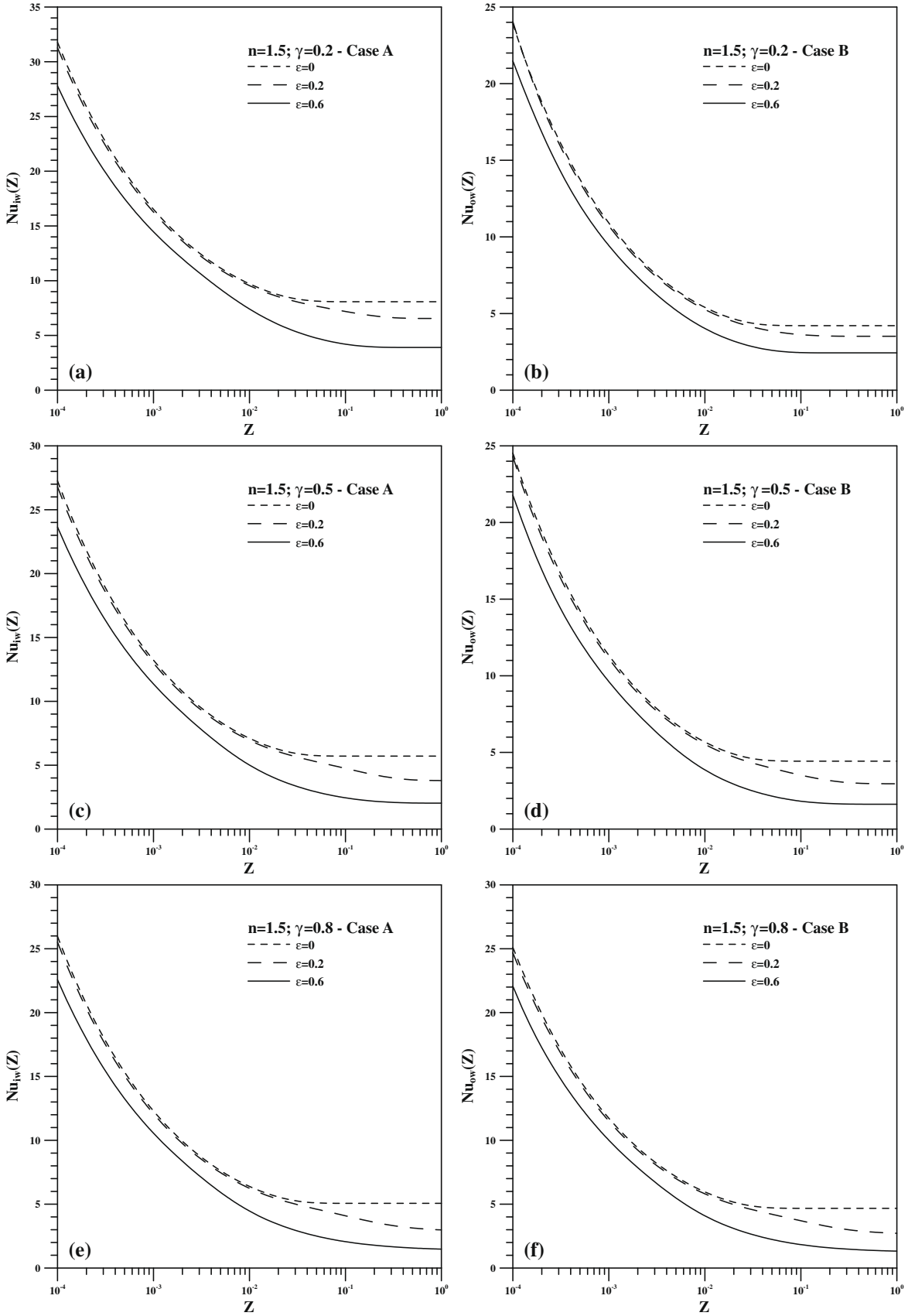

Fig. 8. Evolution of the local Nusselt number along the thermal entry region for $n = 1.5$ and different eccentricities: (a) $\gamma = 0.2$ – Case A; (b) $\gamma = 0.2$ – Case B; (c) $\gamma = 0.5$ – Case A; (d) $\gamma = 0.5$ – Case B; (e) $\gamma = 0.8$ – Case A; and (f) $\gamma = 0.8$ – Case B.

dimensionless eccentricities and radii ration. Here a typical CPU time is about 600 s as for those computations reported in Table 4.

Table 4 illustrates the convergence behavior of the proposed eigenfunction expansion for the local Nusselt number in the thermal entry region (i.e., $Z = 10^{-4}$, 10^{-2} and 1) for cases A and B, and for $n = 0.5$, $\gamma = 0.8$, $\varepsilon = 0.6$; $n = 1$, $\gamma = 0.5$, $\varepsilon = 0.2$ and $n = 1.5$, $\gamma = 0.2$, $\varepsilon = 0$. It can be observed the excellent convergence rate behavior in all cases analyzed, with practically three converged digits for the position $Z = 10^{-4}$, four digits for $Z = 10^{-2}$, and five digits for Z = 1. The same values for the maximum truncations orders in the double summations, $NT = NT^{*} = 40$, were employed in this convergence analysis, and then employed throughout the computations.

Tables 5a and 5b show a comparison of the asymptotic Nusselt numbers for case A against those of Manglik and Fang [17], and with an analytical solution for $\varepsilon = 0$ based on refs. [39,40] for both cases A and B. It can be noticed the excellent agreement among the present results and those of the analytical solution [39,40], and a fairly good agreement is also verified against the results of Manglik and Fang [17]. Such comparisons for the asymptotic Nusselt number provide a direct validation of the proposed approach and developed computational codes in the present work.

Fig. 5 present the distribution of the temperature ratio T/T_m, for the fully developed region, at $\theta = 0^{o}$ and $\theta = 180^{o}$ as a function of the normalized radial coordinate, R_n, for different power-law indices, eccentricities and radii ratio $\gamma = 0.5$, directly comparing side by side the behavior of the two configurations of boundary conditions, cases A and B. In each set of figures (Fig. 5)a–d we also vary the power law index $n = 0.5$, 1.0 and 1.5, and the eccentricity, $\varepsilon = 0$, 0.2 and 0.6. In general, the temperature ratio T/T_m levels are larger for case B, fixing all the governing parameters, in light of the larger surface area available at the external wall in comparison to case A, when the active heat transfer surface is the internal one.

Finally, Figs. 6–8 bring the development of the local Nusselt number along the thermal entry region of the channel, for different power-law indices, $n = 0.5$, 1.0 and 1.5, respectively, and different values of radii ration and eccentricities. The Nusselt number is computed at the internal wall for case A, and at the external wall for case B, and this set of curves provides reference results for the Nusselt number development within eccentric circular channels. The effect of the boundary condition shows that the local Nusselt numbers are higher for case A, with heat transfer at the internal wall of smaller surface area, and the power-law index effect is more pronounced for $n = 0.5$. The radii ratio influence shows that the Nusselt number tends to a more symmetrical distribution for higher radii ratio (cases A and B tend to the same values as the parallel plates configuration is approached), while the eccentricity increase results in lower values of the local Nusselt number.

4. Conclusions

A solution based on the Generalized Integral Transform Technique – GITT was developed to predict fully developed and thermally developing laminar flow of non-Newtonian power-law fluids in doubly connected ducts. The proposed integral transform approach provided reliable and cost effective simulations for the considered case of an eccentric circular channel, by employing a cylindrical coordinates representation of the solution domain. The case of eccentric annular duct was more closely analyzed, and benchmark results for the velocity and temperature fields, as well as for quantities of practical interest such as the product of the Fanning friction factor-Reynolds number, average temperature and local Nusselt numbers were systematically tabulated or graphically shown for different values of the governing geometric parameters, demonstrating the usefulness and robustness of the GITT alternative solution procedure. The good agreement of the present results with those in the literature also served to demonstrate the ability of the integral transform approach in handling such class of problems, under the here introduced domain representation and eigenfunction expansion proposition. The effects of power-law index, eccentricity and radii ratio were also noticed on the product *fRe* and on the local Nusselt number.

Acknowledgements

The authors acknowledge the financial support provided by CNPq during the pos-doctoral fellowship of Professor J.N.N. Quaresma at the Laboratory of Transmission and Technology of Heat, Mechanical Engineering Department, Universidade Federal do Rio de Janeiro.

References

[1] R.K. Shah, A.L. London, Laminar Flow Forced Convection in Ducts, Academic Press, New York, 1978.
[2] R.K. Shah, M.S. Bhatti, Laminar convective heat transfer in ducts, in: S. Kakaç, R.K. Shah, W. Aung (Eds.), Handbook of Single-Phase Convective Heat Transfer, Wiley–Interscience, New York, 1987. pp. 3.1–3.137.
[3] M.A. Ebadian, Z.F. Dong, Forced convection, internal flow in ducts, in: W.M. Rohsenow, J.P. Hartnett, Y.I. Cho (Eds.), Handbook of Heat Transfer, third ed., McGraw-Hill, New York, 1998. pp. 5.1–5.137.
[4] N.A.V. Piercy, M.S. Hooper, H.F. Winny, Viscous flow through pipes with cores, London Edinburgh Dublin Philosophical Magazine, J. Sci. 15 (1933) 647–676.
[5] U.A. Sastry, Heat transfer by laminar forced convection in multiply connected cross-section, Indian J. Pure Appl. Phys. 3 (1965) 113–116.
[6] U.A. Sastry, Viscous flow through tubes of doubly connected regions, Indian J. Pure Appl. Phys. 3 (1965) 230–232.
[7] P.N. Shivakumar, Viscous flow in pipes whose cross-sections are doubly connected regions, Appl. Sci. Res. Sect. A 27 (1973) 355–365.
[8] H.C. Topakoglu, O.A. Arnas, Convective heat transfer for steady laminar flow between to confocal elliptical pipes with longitudinal uniform wall temperature gradient, Int. J. Heat Mass Transfer 17 (1974) 1487–1498.
[9] C. Stevenson, The centre of flexure of a hollow shaft, Proc. Lond. Math. Soc., Ser. 2 50 (1949) 536.
[10] W.T. Snyder, G.A. Goldstein, An analysis of fully developed laminar flow in an eccentric annulus, AIChE J. 11 (1965) 462–467.
[11] V.K. Jonsson, E.M. Sparrow, Results of laminar flow analysis and turbulent flow experiments for eccentric annular duct, AIChE J. 11 (1965) 1143–1145.
[12] K.C. Cheng, G.J. Hwang, Laminar forced convection in eccentric annuli, AIChE J. 14 (1968) 510–512.
[13] M.L. Trombetta, Laminar forced convection in eccentric annuli, Int. J. Heat Mass Transfer 14 (1971) 1161–1173.
[14] K. Suzuki, J.S. Szmyd, H. Ohtsuka, Laminar forced convection heat transfer in eccentric annuli, Heat Transfer-Jpn. Res. 20 (1991) 169–183.
[15] R.M. Manglik, P.P. Fang, Effect of eccentricity and thermal boundary conditions on laminar fully developed flow in annular ducts, Int. J. Heat Fluid Flow 16 (1995) 298–306.
[16] P.P. Fang, R.M. Manglik, M.A. Jog, Characteristics of laminar viscous shear-thinning fluid flows in eccentric annular ducts, J. Non-Newtonian Fluid Mech. 84 (1999) 1–17.
[17] R.M. Manglik, P.P. Fang, Thermal processing of viscous non-Newtonian fluids in annular ducts: effects of power-law rheology, duct eccentricity and thermal boundary conditions, Int. J. Heat Mass Transfer 45 (2002) 803–814.
[18] M.P. Escudier, P.J. Oliveira, F.T. Pinho, Fully developed laminar flow of purely viscous non-Newtonian liquids through annuli, including the effects of eccentricity and inner-cylinder rotation, Int. J. Heat Fluid Flow 23 (2002) 52–73.
[19] P.M. Coelho, F.T. Pinho, Fully-developed heat transfer in annuli with viscous dissipation, Int. J. Heat Mass Transfer 49 (2006) 3349–3359.
[20] F.T. Pinho, P.M. Coelho, Fully-developed heat transfer in annuli for viscoelastic fluids with viscous dissipation, J. Non-Newtonian Fluid Mech. 138 (2006) 7–21.
[21] J.B. Aparecido, R.M. Cotta, M.N. Özişik, Analytical solutions to two-dimensional diffusion type problems in irregular geometries, J. Franklin Inst. 326 (1989) 421–434.
[22] J.B. Aparecido, R.M. Cotta, Laminar flow inside hexagonal ducts, Comput. Mech. 6 (1990) 93–100.
[23] F.A.A. Barbuto, R.M. Cotta, Integral transformation of elliptic problems within irregular domains – fully developed channel flow, Int. J. Numer. Methods Heat Fluid Flow 7 (1997) 778–793.
[24] R.M. Cotta, Integral Transforms in Computational Heat and Fluid Flow, CRC Press, Boca Raton, FL, 1993.
[25] R.M. Cotta, Hybrid numerical–analytical approach to nonlinear diffusion problems, Numer. Heat Transfer Part B 127 (1990) 217–226.
[26] R.M. Cotta, M.D. Mikhailov, Hybrid methods and symbolic computations, in: W.J. Minkowycz, E.M. Sparrow, J.Y. Murthy (Eds.), Handbook of Numerical Heat Transfer, second ed., Wiley, New York, 2006. pp. 493–522.

[27] J.B. Aparecido, R.M. Cotta, Thermally developing laminar flow inside rectangular ducts, Int. J. Heat Mass Transfer 33 (1990) 341–347.
[28] J.B. Aparecido, R.M. Cotta, Laminar thermally developing flow inside right triangular ducts, Appl. Sci. Res. 49 (1992) 355–368.
[29] C.L. Chaves, J.N.N. Quaresma, E.N. Macêdo, L.M. Pereira, J.A. Lima, Hydrodynamically developed laminar flow of non-Newtonian fluids inside double-sine ducts, Hybrid Methods Eng. 3 (2001) 1–14.
[30] C.L. Chaves, J.N.N. Quaresma, E.N. Macêdo, L.M. Pereira, J.A. Lima, Forced convection heat transfer to power-law non-Newtonian fluids inside triangular ducts, Heat Transfer Eng. 25 (2004) 23–33.
[31] J.N.N. Quaresma, E.R. Monteiro, C.L. Chaves, E.N. Macêdo, R.M. Cotta, Thermally developing flow of power law non-Newtonian fluids in double-sine ducts, in: Proceedings of the 13th International Heat Transfer Conference, Sidney, Australia, 2006.
[32] C.R.M. Maia, J.B. Aparecido, L.F. Milanez, Heat transfer in laminar flow of non-Newtonian fluids in ducts of elliptical section, Int. J. Therm. Sci. 45 (2006) 1066–1072.
[33] L.A. Sphaier, R.M. Cotta, Integral transform analysis of multidimensional eigenvalue problems within irregular domains, Numer. Heat Transfer Part B 38 (2000) 157–175.
[34] R.B. Bird, R.C. Armstrong, O. Hassager, Dynamics of Polymeric Liquids, second ed., vol. 1, Wiley, New York, 1987.
[35] IMSL MATH/LIBRARY, User's Manual, Version 2.0, IMSL, Houston, 1991.
[36] M.D. Mikhailov, M.N. Özişik, Unified Analysis and Solutions of Heat and Mass Diffusion, Wiley, New York, 1984.
[37] E.J. Correa, R.M. Cotta, H.R.B. Orlande, On the reduction of computational costs in eigenfunction expansions of multidimensional diffusion problems, Int. J. Numer. Methods Heat Fluid Flow 7 (1997) 675–695.
[38] H.A. Machado, R.M. Cotta, Analysis of internal convection with variable physical properties via integral transformation, Numer. Heat Transfer Part A 36 (1999) 699–724.
[39] M.J.G. Viana, U.C.S. Nascimento, J.N.N. Quaresma, E.N. Macêdo, Integral transform method for laminar heat transfer convection of Herschel–Bulkley fluids within concentric annular ducts, Braz. J. Chem. Eng. 18 (2001) 337–358.
[40] U.C.S. Nascimento, E.N. Macêdo, J.N.N. Quaresma, Thermal entry region analysis through the finite integral transform technique in laminar flow of Bingham fluids within concentric annular ducts, Int. J. Heat Mass Transfer 45 (2002) 923–929.